Bull. Mater. Sci., Vol. 34, No. 3, June 2011, pp. 463–468. © Indian Academy of Sciences.

Magnetic and microwave-absorbing properties of $SrAl_4Fe_8O_{19}$ powders synthesized by coprecipitation and citric-combustion methods

H Y HE*, J F HUANG, L Y CAO, Z HE and Q SHEN

Key Laboratory of Auxiliary Chemistry & Technology for Chemical Industry, Ministry of Education, Shaanxi University of Science and Technology, Xi'an, Shaanxi 710021, China

MS received 12 September 2010; revised 16 January 2011

Abstract. **Al-substituted *M*-type hexaferrite is a highly anisotropic ferromagnetic material. In the present study, the coprecipitation and the citric-combustion methods of synthesis for $SrAl_4Fe_8O_{19}$ powders were explored and their microstructure, magnetic properties, and microwave absorptivity examined. X-ray diffraction (XRD), scanning electron microscopy (SEM), a vibrating sample magnetometer, and a vector network analyser were used to characterize the powders. The XRD analyses indicated that the pure $SrAl_4Fe_8O_{19}$ powder was synthesized at 900°C and 1000°C for 3 h by coprecipitation, but only at 1000°C for the citric-combustion processes. The SEM analysis revealed that the coprecipitation process yielded a powder with a smaller particle size, near single-domain structure, uniform grain morphology, and smaller shape anisotropy than the citric-combustion process. The synthesis technique also significantly affected the magnetic properties and microwave-absorptivity. Conversely, calcining temperature and calcining time had less of an effect. The grain size was found to be a key factor affecting the property of the powder. The powders synthesized by coprecipitation method at calcining temperature of 900°C exhibited the largest magnetization, largest coercivity, and best microwave absorptivity.**

Keywords. **$SrAl_4Fe_8O_{19}$; coprecipitation method; shape anisotropy; magnetic property; microwave absorption.**

1. Introduction

M-type hexaferrites possess excellent magnetic properties, a relatively high magnetocrystalline anisotropic field, and plate-like morphology. This makes this type of ferrite very suitable for microwave materials and microwave absorption. Certain cation substitutions have been shown to further change the anisotropy such as the Al substituted Ba-hexaferrite powder and Sr-hexaferrite film prepared by Choi *et al* (2003) and Heczko *et al* (2000). When rate of Al-substitution reached 4, the magnetocrystalline anisotropic field (H_k) of the ferrite reached a maximum value about three times higher than the pure one (Choi *et al* 2003). In addition, it is generally believed that the microwave response frequency (ωk) of the ferrite increases with increase in H_k ($\omega k = \gamma H_k$, where γ is gyromagnetic ratio). Thus, $SrAl_4Fe_8O_{19}$ ferrite might be a promising high frequency microwave material and high frequency microwave absorber. However, wet chemical synthesis and microwave property of the Al-substituted *M*-type ferrite were rarely reported in literature.

The properties of the substituted hexaferrites are largely dependent on their characteristics such as anisotropy, crystallinity, particle size, and substitution rate. Many process routes have been devised for the preparation of hexaferrite powders with refined particle size, narrow particle-size distribution, minimal particle agglomeration, and high crystallinity, including the hydrothermal process (Komarneni *et al* 1998), the microemulsion technique (Pankov 1997), and the coprecipitation route (Kreisel *et al* 2001). In recent years, the sol–gel combustion process has been widely studied for the synthesis of this type of ferrite powders (Wang *et al* 1996; Han *et al* 2009; Sablea *et al* 2009; Chen *et al* 2010). Various chelating agents have been explored for the formation of homogenous, stable, and transparent sol solutions, and likewise, various reducing agents such as citric acid (Han *et al* 2009; Chen *et al* 2010), stearic acid (Wang *et al* 1996) glycine, and urea (Sablea *et al* 2009) have been studied to find out the one that supplies the requisite energy to initiate the exothermic reaction amongst oxidants. These studies are important since the synthesis route can affect the characteristics of the synthesized powders. In this study, a comparison was made of the formation, particle morphology, anisotropy, magnetic properties, and microwave-absorptivities between Al-substituted Sr-hexaferrite powders

*Author for correspondence (hehy@sust.edu.cn)

synthesized by the coprecipitation method and by the citric sol–gel combustion method.

2. Experimental

2.1 *Coprecipitation*

Ferric nitrate ninhydrate, strontium chloride dihydrate, and aluminium chlorite hexahydrate were dissolved with stirring in distilled water, with the resulting molarities being 0·05 M for Sr^{2+}, 0·20 M for Al^{3+}, and 0·40 M for Fe^{3+}. Then, a sodium hydroxide aqueous solution was slowly added dropwise into the solution at room temperature with constant stirring condition until pH = 9–10. When the coprecipitation was complete, the precipitate slurry was filtrated and washed with anhydrous ethanol until pH∼7, and then dried at 100°C for 10 h. After preheating the precursor at 300°C for 1 h, the precursor was heated in a furnace at a rate of 25°C·min^{-1} and then calcined at 900°C or 1000°C for 3 h. Cooling process was naturally performed in furnace.

2.2 *Citric-combustion*

The ferric nitrate ninhydrate, strontium chloride dihydrate, aluminium nitrate hexahydrate were dissolved in distilled water containing citric acid by stirring for 0·5 h. The solution had molarities of 0·05 M for Sr^{2+}, 0·20 M for Al^{3+}, and 0·40 M for Fe^{3+}. The molar ratio of metal cations to citric acid was 1:1·5. The pH of the solution was adjusted by slowly adding aqueous ammonia with constant stirring until pH = 7–8. The solution was then dried at 80°C or 100°C for 24 h. After drying, the samples were heated at a rate of ∼25°C·min^{-1}, and the combustion took place at ∼250°C. After maintaining a temperarture of 250–300°C for 1 h, the precursor was heated in a furnace at the rate of 25°C·min^{-1} and calcined at 900°C and 1000°C for 3 h and 5 h, respectively. Cooling process was naturally performed in furnace.

2.3 *Sample analysis*

DSC/TG patterns of dried citric gel were analysed using a simultaneous TG-DTA/DSC apparatus (TG-DTA/DSC, Model No. STA409PC, Netzsch, Germany) in a N_2 atmosphere at a heating rate of 10°C/min. The phase of the synthesized ferrite powders was identified at room temperature using a X-ray diffractometer (XRD, $CuK_{\alpha 1}$, λ = 0·15406 nm, Model No. D/Max-2200PC, Rigaku, Japan). Scanning electron microscopy (SEM, Model No. JXM-6700F, Japan) was used to analyse the particle morphology of the powder. The magnetic property was measured with a vibrating sample magnetometer (VSM, Model No. Versa Lab, Quantun Design, USA), and variation of the reflection loss in (dB) versus frequency was investigated in the range of 10–20 GHz with a vector network analyser (Model No. N5230A, USA). For measuring reflection loss, the ferrites were mixed with an aqueous polyvinyl alcohol (20 wt%) and stirred for 1 h. Specimens with a thickness of 1·5 mm were finally formed by cold isostatic pressing of 100 MPa.

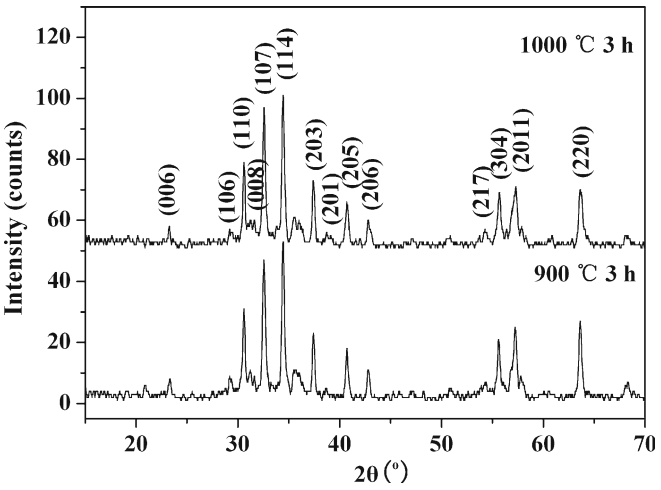

Figure 1. XRD patterns of $SrAl_4Fe_8O_{19}$ powder synthesized by co-precipitation.

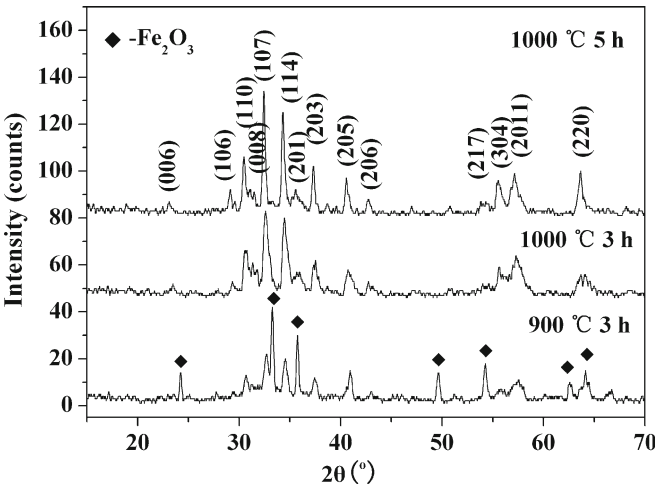

Figure 2. XRD patterns of $SrAl_4Fe_8O_{19}$ powder synthesized by citric-combustion method.

3. Results and discussion

Figures 1 and 2 illustrate XRD patterns of the powders synthesized by coprecipitation and citric-combustion methods, respectively. The samples synthesized by coprecipitation all have a pure $SrAl_4Fe_8O_{19}$ phase when the precursor was calcined at 900°C and 1000°C. For the citric-combustion samples, the samples calcined at 1000°C for 3 h and 5 h were pure $SrAl_4Fe_8O_{19}$ phase; the samples calcined at 900°C for

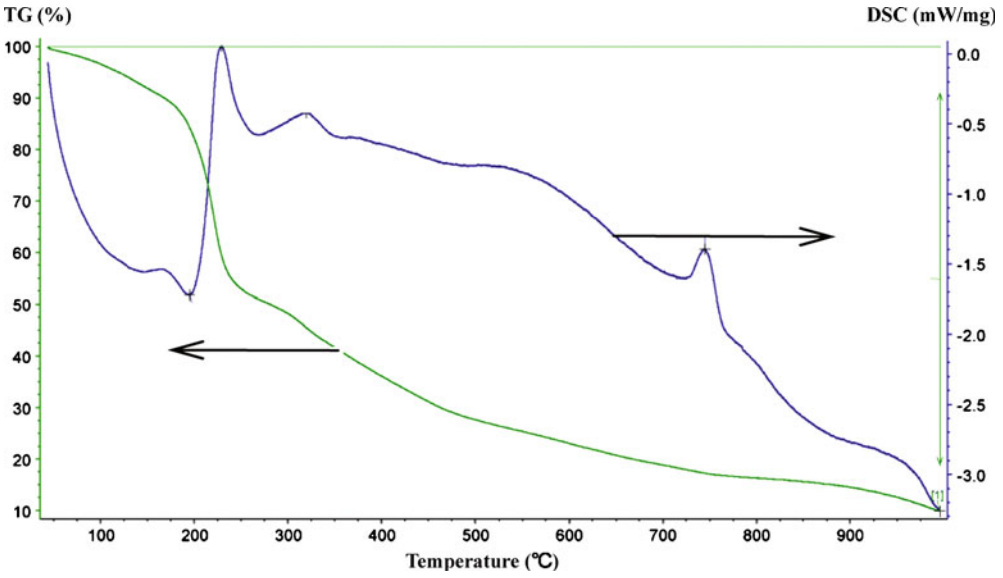

Figure 3. TG/DSC of citric acid gel containing metal cations.

5 h were Fe_2O_3 phase. In this study, the pure $SrAl_4Fe_8O_{19}$ phase was obtained at 1000°C for the longer time of 3 h compared to the 5 h reported in literature (Wang *et al* 1996; Han *et al* 2009). The TG/DSC curves of dried citric gel indicated that the gel still exhibited endothermic and agravic tendencies until 950°C (figure 3). This feature could have resulted from the decomposition of the $SrCO_3$, which may be the reason why the citric-combustion synthesis route for $SrAl_4Fe_8O_{19}$ required a higher calcining temperature.

The lattice constants of the powders were calculated using the d, h, k, and l values of the strong (110), (008), (107), (114), (203), (2011), and (220) peaks in the XRD patterns according to the equation

$$\frac{a^2}{d^2} = \frac{4}{3}\left(h^2 + hk + k^2\right) + l^2\frac{a^2}{c^2}.$$

The unit cell volume (V_{cell}) of the hexagonal system was calculated as follows

$$V_{cell} = 0{\cdot}866a^2c,$$

where the numeric factor is constant for the hexagonal system. As calculated, the lattice parameters a, c, V_{cell} and c/a ratio of the $SrAl_4Fe_8O_{19}$ powders are listed in table 1. The a, c and V_{cell} value of the substituted ferrite powders were smaller than that of pure $SrFe_{12}O_{19}$ (PDF#33-1340) while the c/a ratios of the substituted ferrite powders were larger. These agree with the result reported by Choi *et al* (2003). The lattice parameter changes with the Al-substitution could be attributed to the smaller ionic radius of Al^{3+} (0·50 Å) compared with Fe^{3+} (0·64 Å). Additionally, the V_{cell} value decreased as calcining temperature increased for the coprecipitation-derived powders and as the calcining time increased for the sol–gel-derived powders. The lower calcining temperature for coprecipitation and longer calcining time for citric-combustion led to an increase of c/a value.

In figure 4, the powder synthesized by coprecipitation had a smaller particle size near the single-domain, smaller shape anisotropy, and a more uniform plate-like morphology. With the increasing calcining temperature, the shape anisotropy

Table 1. Lattice parameter of $SrAl_4Fe_8O_{19}$ powders determined from XRD data analysis, and average grain size of the powders determined from SEM analysis.

Sample	Lattice parameter				Average grain size (nm)
	a (Å)	c (Å)	c/a	V_{cell} (Å^3)	
Coprecipitation method					
900°C 3 h	5·8376	22·9781	3·9362	678·1108	55
1000°C 3 h	5·8364	22·9593	3·9339	677·2775	61
Citric-combustion method					
1000°C 3 h	5·8469	22·9524	3·9255	679·5123	130
1000°C 5 h	5·8515	23·0547	3·9399	673·6153	165
$SrFe_{12}O_{19}$ (PDF#33-1340)	5·887	23·037	3·913	691·404	

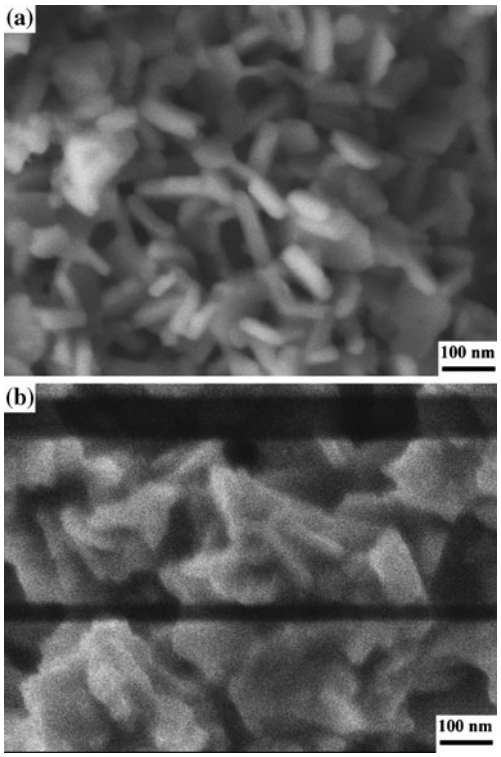

Figure 4. SEM micrographs of $SrAl_4Fe_8O_{19}$ powders synthesized by co-precipitation method. The powders were calcined at **(a)** 900°C and **(b)** 1000°C for 3 h.

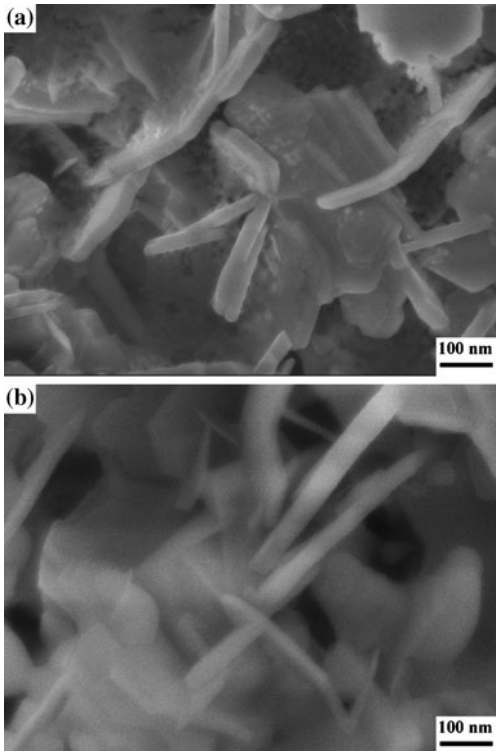

Figure 5. SEM micrographs of $SrAl_4Fe_8O_{19}$ powder synthesized by citric-combustion method. The powders were calcined at 1000°C for **(a)** 3 h and **(b)** 5 h.

and average grain size slightly increased. However, figure 5 indicates that the powder synthesized by citric-combustion had a larger particle size, a non-uniform plate-like morphology, and a larger shape anisotropy. As the calcining time increased though, the shape anisotropy decreased. The powder consisted of large grains up to 170–200 nm in size as well as small grains, and the average grain size appeared to increase with increasing calcining time.

Figure 6 shows the room temperature hysteresis loops of the powders synthesized by the coprecipitation method. The magnetization of the powders synthesized at 900°C and 1000°C were 30·50 emu·g^{-1} and 28·49 emu·g^{-1} respectively. The easy axis of magnetization was parallel to the hexagonal *c*-axis and is described by the anisotropy constant K_1. Thus, a calcining temperature of 900°C could yield a more intense crystal growth in the *c*-axis than 1000°C, which would result in the decrease in magnetization with increasing calcining temperature (figure 4). The coercivity was 9·07 ± 0·04 kOe and 8·51 ± 0·04 kOe, respectively for the powders calcined at 900°C and 1000°C. In general, magneto-crystalline anisotropy and grain size determine the possible coercivity, with maximum coercivity at the single-domain size. This could explain the slight decrease in coercivity with calcining temperature because of the increase in average grain size (table 1).

The powders synthesized by the citric-combustion method exhibited similar magnetic trends (figure 7). The magneti-

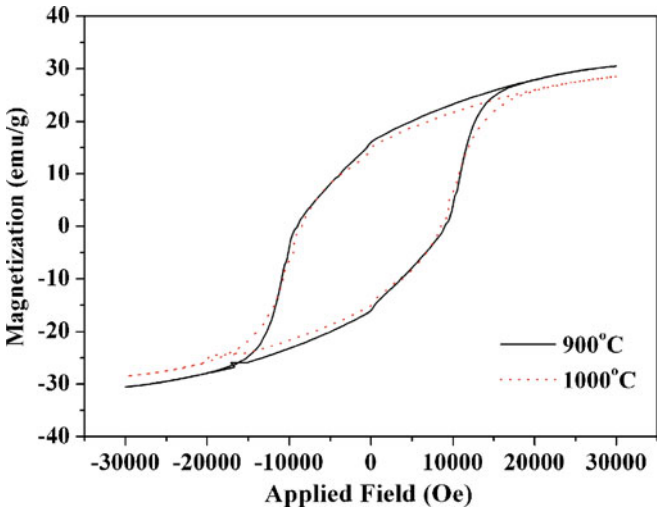

Figure 6. Room temperature hysteresis loops of $SrAl_4Fe_8O_{19}$ powder synthesized by co-precipitation method.

zation of the powders calcined for 3 h and 5 h were 23·90 emu·g^{-1} and 23·16 emu·g^{-1}, and the coercivity was 2·19 ± 0·04 kOe and 0·45 ± 0·04 kOe, respectively for the powders calcined for 3 h and 5 h. As with the results for the co-precipitation method, these results were likely due to preferred growth in the *c*-axis for the magnetization (figure 5)

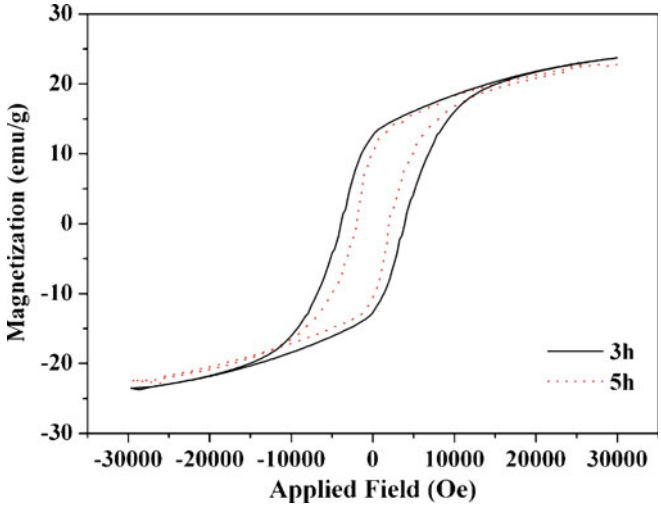

Figure 7. Room temperature hysteresis loops of $SrAl_4Fe_8O_{19}$ powder synthesized by citric-combustion method.

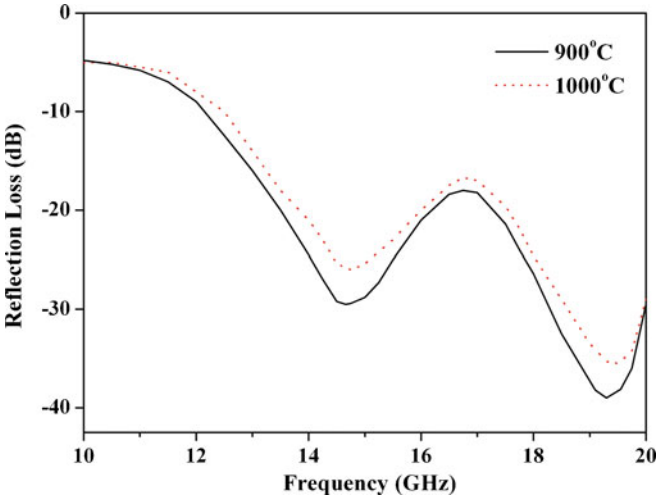

Figure 8. Variation of reflection loss of $SrAl_4Fe_8O_{19}$ powder synthesized by co-precipitation method vs frequency.

and average grain size and anisotropy for the coercivity (table 1).

With increasing rate of Al-substitution, the saturation magnetization of *M*-type ferrite increases while the coercivity decreases. In view of this, the saturation magnetization and the coercivity of the $BaAl_4Fe_8O_{19}$ powders synthesized by the coprecipitation were respectively larger than and close to 30·2 emu·g^{-1} and 8·7 kOe of $BaFe_{10}Al_2O_{19}$ observed under an applied field of 15 kOe as reported by Choi *et al* (2003). The saturation magnetization and the coercivity of the powders synthesized by the citric-combustion method might be respectively close to and smaller than the value reported by Choi *et al* (2003).

Comparing the two methods of synthesis, the magnetizations and coercivities of the powders synthesized by citric-combustion were smaller than those of the powders synthesized by coprecipitation. The first could be due to the smaller single-domain grain size in the powders synthesized by citric-combustion method (figure 5), and the second could be attributed to the nonuniform morphology of the powders consisting of the grains larger and smaller than the single-domain size; there seemed to be no obvious dependence in anisotropy.

Figures 8 and 9 show the variation in reflection loss of the powders vs frequency. The ferromagnetic resonance frequency (f_r) of ferrite can be given by following relation:

$$2\pi f_r = \gamma\sqrt{H_\theta H_\phi}.$$

This equation states that the ferromagnetic resonance frequency is related to the magnetocrystalline anisotropy fields H_θ and H_ϕ of ferrites. All samples showed two ferromagnetic resonance peaks in the range of 10–20 GHz, corresponding to the domain wall motion at the lower frequency and spin resonance at the higher frequency. The bandwidth of resonance frequency was defined as the frequency width in which the reflection loss was more than −20 dB. The resonance frequency, minimum reflection loss, and bandwidth of the powders are summarized in table 2. By comparison, the powders synthesized by the coprecipition method have higher resonance frequencies, larger reflection loss, and wider bandwidths. This could be attributed to their uniform grain morphology and small grain size close to the single-domain. The powder synthesized by the coprecipitation method at a calcining temperature of 900°C had the largest reflection loss value of −39·0 dB and widest bandwidth of 4·4 GHz at the higher matching resonance frequency of 19·30 GHz, and thus demonstrated the best microwave-absorbing properties.

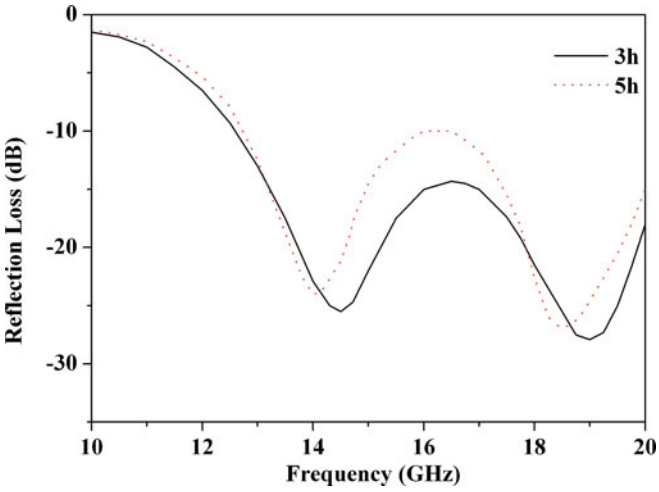

Figure 9. Variation of reflection loss of $SrAl_4Fe_8O_{19}$ powder synthesized by citric-combustion method vs frequency.

Table 2. Resonance frequency (f_r), minimum reflection loss (RL_{min}) and bandwidth ($RL_{min} < -20$ dB) of $SrAl_4Fe_8O_{19}$ powders.

Sample	f_r(GHz)	RL_{min}(dB)	Bandwidth (GHz)
Coprecipitation method			
900°C	14·66	−29·5	2·8
	19·30	−39·0	4·4
1000°C	14·75	−26·0	2·1
	19·51	−35·5	4·0
Citric-combustion method			
3 h	14·47	−14·5	1·6
	19·03	−27·9	1·9
5 h	14·05	−24·0	2·0
	18·47	−27·1	1·8

Chen *et al* (2010) fabricated the pure and La-substituted Sr-ferrite $Sr_{1-x}La_xFe_{12}O_{19}$ ($x = 0$–$0{\cdot}5$) powders by a sol–gel technique followed by an auto-combustion process. The minimum reflection loss of the powders was improved from −24 to −41·7 dB with increasing substitution rate from $x = 0$ to $x = 0{\cdot}15$, but the response frequency was only at ∼9·6 GHz. By comparison, our study indicated that the Al-substitution remarkably increased response frequency of the Sr-ferrite powders.

4. Conclusions

M-type $SrAl_4Fe_8O_{19}$ powders were synthesized by the coprecipitation method and the citric-combustion method. The synthesis technique greatly affected the microstructure, the magnetic property, and the microwave absorptivity of the $SrAl_4Fe_8O_{19}$ powders. Comparatively, calcining temperature and calcining time had little effect on these properties. The powders synthesized by the coprecipitation method had uniform grain morphology, smaller grains near the single-domain size, and smaller shape anisotropy, and exhibited larger magnetization, larger coercivity, and better microwave-absorptivity compared to the powders synthesized by citric-combustion method. The grain size was found to be an important factor in determining these properties of the powders. By selecting the appropriate synthesis technique, the $SrAl_4Fe_8O_{19}$ powder can be an effective microwave absorber for over 14 GHz with satisfactory reflection loss.

Acknowledgements

The authors thank Mr Z Miao, Northwest Institute for Non-Ferrous Metal Research, for his kind assistance in SEM measurement, Mr S Liu, Advanced Material Analysis and Test Centre, Xi'an University of Technology, for his kind assistance in magnetic property and microwave absorption ability measurements, and the financial assistance of the specific scientific research projects of Shaanxi Provincial Education Committee (09KJ348).

References

Chen N, Yang K and Gu M 2010 *J. Alloys Compd.* **490** 609
Choi D H, Lee S W, An S Y, Park S I, Shim I B and Kim C S 2003 *IEEE Trans. Magn.* **39** 2884
Han M, Ou Y, Chen W and Deng L 2009 *J. Alloys Compd.* **474** 185
Heczko O, Gerber R and Šimša Z 2000 *Thin Solid Films* **358** 206
Komarneni S, D'Arrigo M C, Leonelli C, Pellacani G C and Katsuki H 1998 *J. Am. Ceram. Soc.* **81** 3041
Kreisel J, Vincent H, Taeest F, Pate M and Ganne J P 2001 *J. Magn. Magn. Mater.* **224** 17
Pankov V 1997 *Mater. Sci. Eng.* **A224** 101
Sablea S N, Rewatkarb K G and Nanoti V M 2009 *Mater. Sci. Eng.* **B168** 156
Wang X, Li D, Lu L and Wang X 1996 *J. Alloys Compd.* **237** 45